Environmental Research 299 (2026) 124392

Contents lists available at ScienceDirect

Environmental Research

journal homepage: www.elsevier.com/locate/envres

Impacts of climate-driven vegetation changes on air quality over East Asia: Modulation of biogenic VOC emissions and secondary pollutants

Seung-Hee Baek [a], Hyo-Jung Lee [a,b,*], Yu-Jin Jo [b,**], Younha Kim [c], Min-Jun Park [a], Cheol-Hee Kim [a,b]

[a] Department of Atmospheric Science, Pusan National University, Busan, 46241, Republic of Korea
[b] Institute of Environmental Studies, Pusan National University, Busan, 46241, Republic of Korea
[c] International Institute for Applied Systems Analysis, 2361, Laxenburg, Austria

ARTICLE INFO

Keywords:
Leaf area index (LAI)
Biogenic volatile organic compounds (BVOCs)
Biogenic secondary organic aerosols (BSOA)
O_3 formation
WRF-Chem
MEGAN

ABSTRACT

Climate change is reshaping terrestrial ecosystems across East Asia, driving substantial shifts in leaf area index (LAI) and vegetation productivity. These changes in vegetation activity directly affect biogenic volatile organic compound (BVOC) emissions, which in turn influence secondary air pollutants such as ozone (O_3) and biogenic secondary organic aerosols (BSOA). We quantify the impact of LAI variability on regional air quality using the WRF-Chem model coupled with the MEGAN biogenic emissions module. We conducted two simulations for August 2024: a baseline case using default 2003 LAI fields and a sensitivity case incorporating updated satellite-derived LAI for 2024. Satellite observations reveal regionally heterogeneous greening trends across East Asia over the past two decades, driven by climatic and land-use changes. Model results show that LAI variations modulate BVOC emissions, and these emission changes propagate to BSOA and O_3 responses depending on local chemical regimes. By combining model simulations with satellite-derived formaldehyde-to-nitrogen dioxide ratios, we find that the strongest BSOA and O_3 responses occur in suburban transition zones where both vegetation changes and chemical conditions favor BVOC oxidation. In contrast, NO_x-saturated megacities experience weaker responses due to suppressed chemical efficiency and smaller vegetation changes, whereas NO_x-limited regions show muted changes despite substantial vegetation increases because insufficient NO_x constrains O_3 and aerosol production. These results highlight that dynamic vegetation processes significantly influence air quality in East Asia. Incorporating realistic vegetation conditions into emission inventories and chemical transport models will enhance predictability and support more effective air quality management under ongoing climate and ecosystem change.

1. Introduction

Climate change has profoundly altered terrestrial ecosystems, driving substantial shifts in vegetation distribution, productivity, and phenology worldwide (Myneni et al., 1997; Zhu et al., 2016; Chen et al., 2019; Piao et al., 2019; Gao et al., 2020; Sun et al., 2022). The leaf area index (LAI), which represents the total leaf area per unit ground surface (m^2 m^{-2}), is a key biophysical indicator of vegetation structure and function (Myneni et al., 2002; Fang et al., 2019). It is also recognized as an Essential Climate Variable (ECV) due to its critical role in the climate system and its importance for quantifying land–atmosphere interactions (GCOS, 2011). Recent satellite observations have revealed a global increase in LAI, driven by climate change-induced warming and elevated carbon dioxide (CO_2) (Piao et al., 2020; Chen et al., 2024; Zhang et al., 2025), with particularly pronounced greening across mid-to high-latitude regions (Zhu et al., 2016; Chen et al., 2019). Notably, large-scale reforestation programs in China have contributed substantially to this greening, accounting for a major fraction of the global LAI increase (Chen et al., 2019, 2020; Jin et al., 2023).

An increase in LAI enhances photosynthetic activity and ecosystem productivity, which in turn increases emissions of biogenic volatile organic compounds (BVOCs), such as isoprene and monoterpenes, and

* Corresponding author. Department of Atmospheric Sciences, Pusan National University, 2, Busandaehak-ro 63beon-gil, Geumjeong-gu, Busan, 46241, Republic of Korea
** Corresponding author.
E-mail addresses: hyojung@pusan.ac.kr (H.-J. Lee), yujinjo@pusan.ac.kr (Y.-J. Jo).

https://doi.org/10.1016/j.envres.2026.124392
Received 14 December 2025; Received in revised form 24 March 2026; Accepted 30 March 2026
Available online 30 March 2026

alters their spatial distribution (Guenther et al., 2006; Sindelarova et al., 2014; Gu et al., 2017; Gai et al., 2024; Wang et al., 2024). BVOCs act as key precursors of both biogenic secondary organic aerosols (BSOA) and tropospheric ozone (O_3) through complex atmospheric chemical reactions. The oxidation of BVOCs by hydroxyl radical (OH), O_3, and nitrate radical (NO_3) yields low-volatility products that partition into the particle-phase to form BSOA. Concurrently, BVOC oxidation produces peroxy radicals (HO_2 and RO_2) that promote O_3 formation through photochemical cycles in the presence of nitrogen oxides (NO_x) (Atkinson and Arey, 2003; Carlton et al., 2009). Consequently, LAI changes driven by climate warming and large-scale land management may exacerbate air quality degradation by enhancing the formation of these secondary pollutants. However, the atmospheric response to LAI perturbations is highly nonlinear, as BVOC–NO_x–O_3 interactions are modulated by meteorological conditions, chemical regimes, and vegetation characteristics (Fiore et al., 2012; Pullinen et al., 2020; Duan et al., 2023). Therefore, a comprehensive and quantitative assessment of the air quality feedbacks associated with LAI variability is essential to improve our understanding of biosphere–atmosphere–climate interactions.

In atmospheric chemistry and air quality modeling, BVOC emissions are generally estimated using biogenic emission models such as the Model of Emissions of Gases and Aerosols from Nature (MEGAN) (Guenther et al., 2012) and the Biogenic Emission Inventory System (BEIS) (Pierce and Waldruff, 1991; Bash et al., 2016). These models parameterize emission rates as functions of temperature, solar radiation, and vegetation characteristics (Pierce and Waldruff, 1991; Guenther et al., 2012; Bash et al., 2016). However, most studies continue to rely on climatological or static vegetation fields, which fail to capture the substantial changes in vegetation structure and density resulting from climate variability and land-use transitions. Given the strong sensitivity of BVOC emissions to both meteorological and vegetation characteristics, accurately representing these dynamic processes is essential for improving predictions of key air pollutants such as O_3 and fine particulate matter ($PM_{2.5}$).

East Asia, in particular, represents a critical region where rapid industrialization and urbanization have led to severe air pollution with diverse O_3 precursors, while concurrent climate-driven changes in vegetation and ecosystems are altering biogenic emission processes.

Recent studies have suggested that variations in BVOC emissions have played a significant role in the observed upward trends of SOA and O_3 across East Asia (Liu et al., 2019, 2025; Lou et al., 2023; Lyu et al., 2024; Wang et al., 2025).

In this study, we quantify the effects of recent vegetation changes on BVOC emissions and air quality over East Asia by incorporating satellite-derived, time-varying LAI datasets into the MEGAN biogenic emission module coupled with the Weather Research and Forecasting model with Chemistry (WRF-Chem) (Skamarock et al., 2019). This modeling framework allows for a more realistic representation of biosphere–atmosphere feedbacks and provides new insights into how climate-induced greening modulates the formation of secondary pollutants in this rapidly changing region.

2. Materials and methods

2.1. Vegetation datasets

The vegetation inputs required by MEGAN include LAI and vegetation continuous fields (VCF), both derived from MODIS satellite products. In the MEGAN framework, LAI_v (the ratio of LAI to VCF), rather than LAI, is used as the vegetation structural input variable, as it represents the one-sided leaf area per unit vegetated canopy area. We employed the MODIS LAI dataset (MCD15A3H, Collection 6.1; Myneni et al., 2002), which provides 4-day composite LAI fields at 500m resolution from 2002 onward, along with the MODIS VCF dataset (MOD44B, Collection 6.1; Hansen et al., 2003), which supplies annual vegetation cover at 250m resolution beginning in 2000. From these datasets, LAI_v was calculated and applied in the MEGAN module within WRF-Chem, following the standard MEGAN input definition.

2.2. Model description and emission inventories

The WRF-Chem v4.5 (Skamarock et al., 2019), a regional air-quality modeling system, was applied in this study. This online-coupled modeling framework simulates meteorology and atmospheric chemistry in an interactive manner, allowing dynamic interactions between physical and chemical processes (Grell et al., 2005). The model domain encompasses East Asia, including China, the Korean Peninsula, and Japan, with a horizontal resolution of $27 \times 27\ km^2$ and 28 vertical sigma levels (Fig. S1). The National Centers for Environmental Prediction (NCEP) Final (FNL) Operational Global Analysis data (NCEP, 2015), with a spatial resolution of $0.25^\circ \times 0.25^\circ$ and temporal resolution of 6 h, provided initial and boundary conditions for the meteorological fields. Gas-phase processes were simulated using the Regional Atmospheric Chemistry Mechanism (RACM) (Stockwell et al., 1997), and aerosol dynamics were treated with the Modal Aerosol Dynamics Model for Europe integrated with the Volatility Basis Set (MADE/VBS) (Ackermann et al., 1998; Ahmadov et al., 2012). Details of the physical and chemical configuration options are provided in Table S1.

Anthropogenic emissions were derived from the updated Comprehensive Regional Emissions for Atmospheric Transport Experiment, version 3 (CREATEv3) (Woo et al., 2020), which is based on a bottom-up inventory combining the Multiresolution Emission Inventory for China (MEIC) for Chinese sources and the Clean Air Policy Support System (CAPSS) for Korean sources (Kim et al., 2023). Further information on the development and characteristics of this inventory is available in Woo et al. (2020). Biogenic emissions were simulated using the MEGAN (Guenther et al., 2006, 2012) v2.04, which is coupled within WRF-Chem to provide online estimates of BVOCs based on meteorological conditions and vegetation parameters.

2.3. Model sensitivity experiments

By default, the MEGAN module in WRF-Chem uses fixed LAI_v fields from the year 2003 as its input. To investigate the influence of more realistic vegetation conditions, we conducted sensitivity experiments in which the default 2003 LAI_v inputs were replaced with the same MODIS-derived LAI_v fields for 2024. Two simulations were conducted for the same simulation period in August 2024: (i) BASE, using the default 2003 LAI_v, and (ii) LAI24, using the 2024 MODIS-derived LAI_v. Except for the prescribed LAI_v fields, all other model inputs—including meteorology, anthropogenic emissions, land cover, and plant functional type (PFT) distributions—were held constant between the two simulations. The LAI_v fields used in this study represent actual MODIS satellite observations for the analysis year (2024), rather than any projected or future vegetation scenarios. The differences between the two experiments provide quantitative estimates of how changes in LAI_v affect biogenic emissions, particularly BVOCs, and the resulting secondary pollutants such as O_3 and BSOA.

WRF-Chem simulations for this study were conducted for the summer period (June–August 2024). August was selected for detailed analysis because vegetation activity reaches its seasonal maximum while the influence of the East Asian summer monsoon is relatively weak. August also exhibits the lowest accumulated precipitation frequency among the summer months (Fig. S2), providing relatively stable meteorological conditions for isolating the impact of LAI_v changes on BVOC emissions and air quality.

2.4. Ground-based and spaceborne observational data

Surface observations of O_3 and $PM_{2.5}$ were obtained from air quality monitoring stations operated by the National Institute of Environmental Research (NIER) in South Korea, where standard quality assurance (QA) and quality control (QC) procedures are applied prior to data release. Hourly data were further screened to remove missing or invalid values before use for model evaluation. The WRF-Chem simulations showed good agreement with observations for both O_3 (R = 0.87, IOA = 0.72) and $PM_{2.5}$ (R = 0.83, IOA = 0.80).

The TROPOspheric Monitoring Instrument (TROPOMI), onboard the Sentinel-5 Precursor satellite, provides daily global observations of key trace gases at high spatial resolution from a sun-synchronous orbit with an equatorial overpass at 13:30 local time (Veefkind et al., 2012; Lorente et al., 2021). The nadir spatial resolution was 3.5 × 7 km^2 at launch and was improved to 3.5 × 5.5 km^2 after August 2019 (van Geffen et al., 2019). In this study, we used tropospheric column densities of nitrogen dioxide (NO_2) and formaldehyde (HCHO). A QA procedure and cloud fraction (CF) filtering were applied, retaining retrievals with QA values greater than 0.5 and excluding those with CF values exceeding 0.3. From these data, the formaldehyde-to-nitrogen dioxide ratio (FNR, defined as $HCHO/NO_2$) was derived and used as an indicator of O_3 formation regimes (Duncan et al., 2010).

3. Results and discussion

3.1. Long-term trends of LAI and LAI_v in East Asia

Fig. 1 presents the long-term variability of LAI and LAI_v over East Asia derived from MODIS satellite products for August during the period from 2003 to 2024. The temporal analysis indicates a significant positive trend in LAI, with an average increase of 0.23 % yr^{-1}, leading to an overall enhancement of approximately 18.4 % by 2024 relative to 2003. In addition, LAI_v exhibits a marginal increase of 0.03 % yr^{-1}, corresponding to a total change of 13.5 % over the same period. These results highlight a widespread increase in vegetation activity across East Asia, consistent with previous studies that reported strong greening trends in the region (Piao et al., 2015; Chen et al., 2019). The spatial distribution of the trends further illustrates the heterogeneous patterns of vegetation change (Fig. 1b). Overall, East Asia exhibits a clear greening signal. In northwestern China, strong increases are evident, consistent with afforestation initiatives and irrigation programs (Piao et al., 2015; Chen et al., 2019). By contrast, parts of northeastern China show negative trends in both LAI and LAI_v, which may be attributed to climatic stressors such as declining soil moisture and reduced precipitation (Cheng et al., 2015; Han et al., 2020). The spatial pattern of LAI_v trends is broadly consistent with that of LAI but exhibits stronger magnitudes, as normalization by VCF amplifies the variations. These heterogeneous responses underscore that vegetation dynamics in the region are jointly shaped by climatic variability and human activities.

To further assess how these observed changes are represented in the model framework, we compared LAI_v fields from the BASE (2003) and LAI24 (2024) experiments, where MODIS-derived vegetation inputs were provided to WRF-Chem/MEGAN. Building on these observationally derived trends, Fig. 2 compares the MODIS fields with the corresponding WRF-Chem/MEGAN vegetation inputs to assess the extent to which the model representation captures the observed variability. Both MODIS and WRF-Chem/MEGAN show consistent spatial patterns, with widespread greening over China and declining trends over the Korean Peninsula and Japan. While MODIS captures fine-scale spatial variability at its native ~500 m resolution, the WRF-Chem/MEGAN derived fields appear smoother and less detailed due to regridding to the coarser WRF-Chem resolution. As a result, the model outputs reproduce the overall greening patterns but underrepresent regional heterogeneity. Nevertheless, the broad-scale agreement between the two datasets indicates that the MEGAN-derived vegetation fields reasonably capture the long-term greening trends.

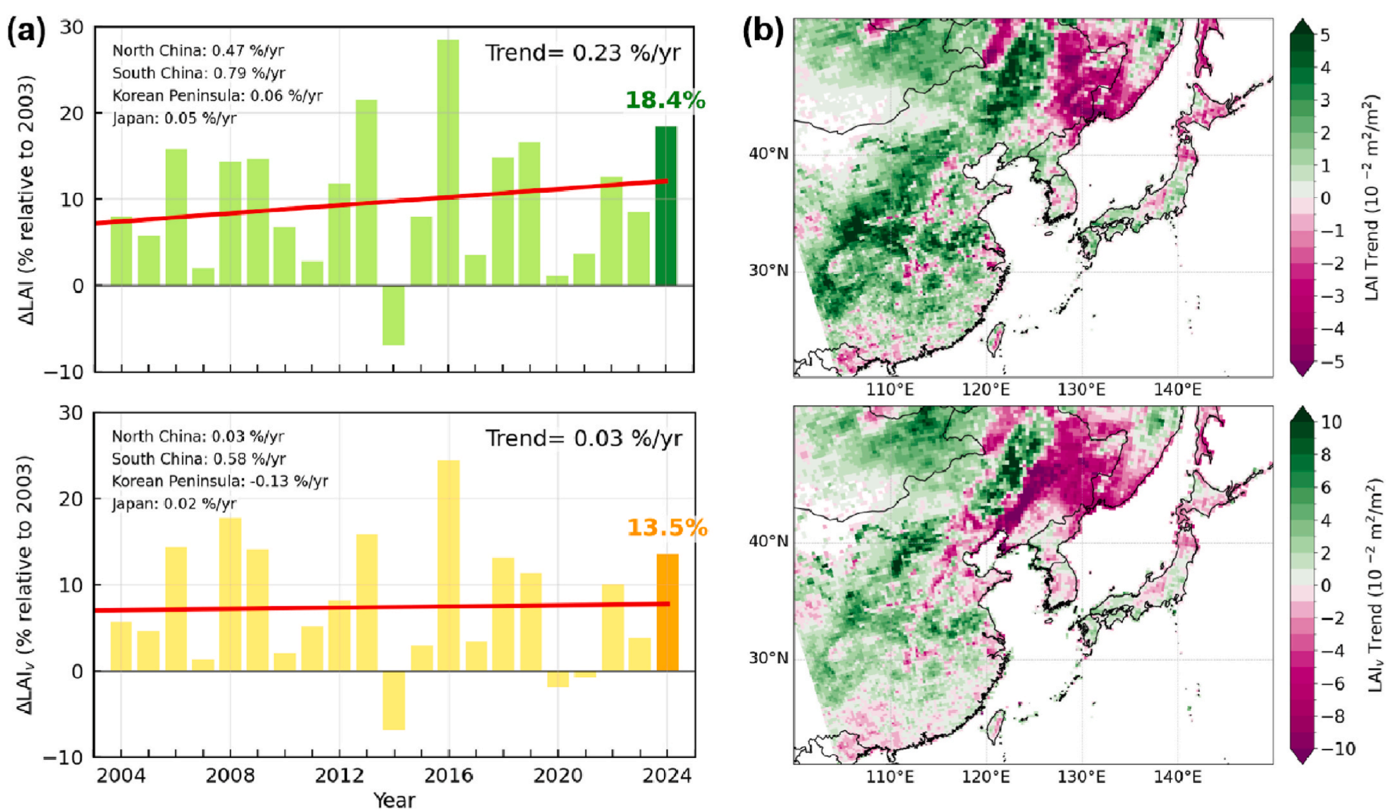

Fig. 1. Long-term variability and trends of LAI and LAI_v over East Asia during August from 2003 to 2024 derived from MODIS. (a) Annual anomalies relative to 2003 with linear regression trends, with 2024 values highlighted to illustrate recent change relative to the baseline year. Regional linear trends for North China, South China, the Korean Peninsula, and Japan are also shown. (b) Spatial distribution of linear trends during 2003–2024, regridded to the WRF-Chem model grid resolution (27 km).

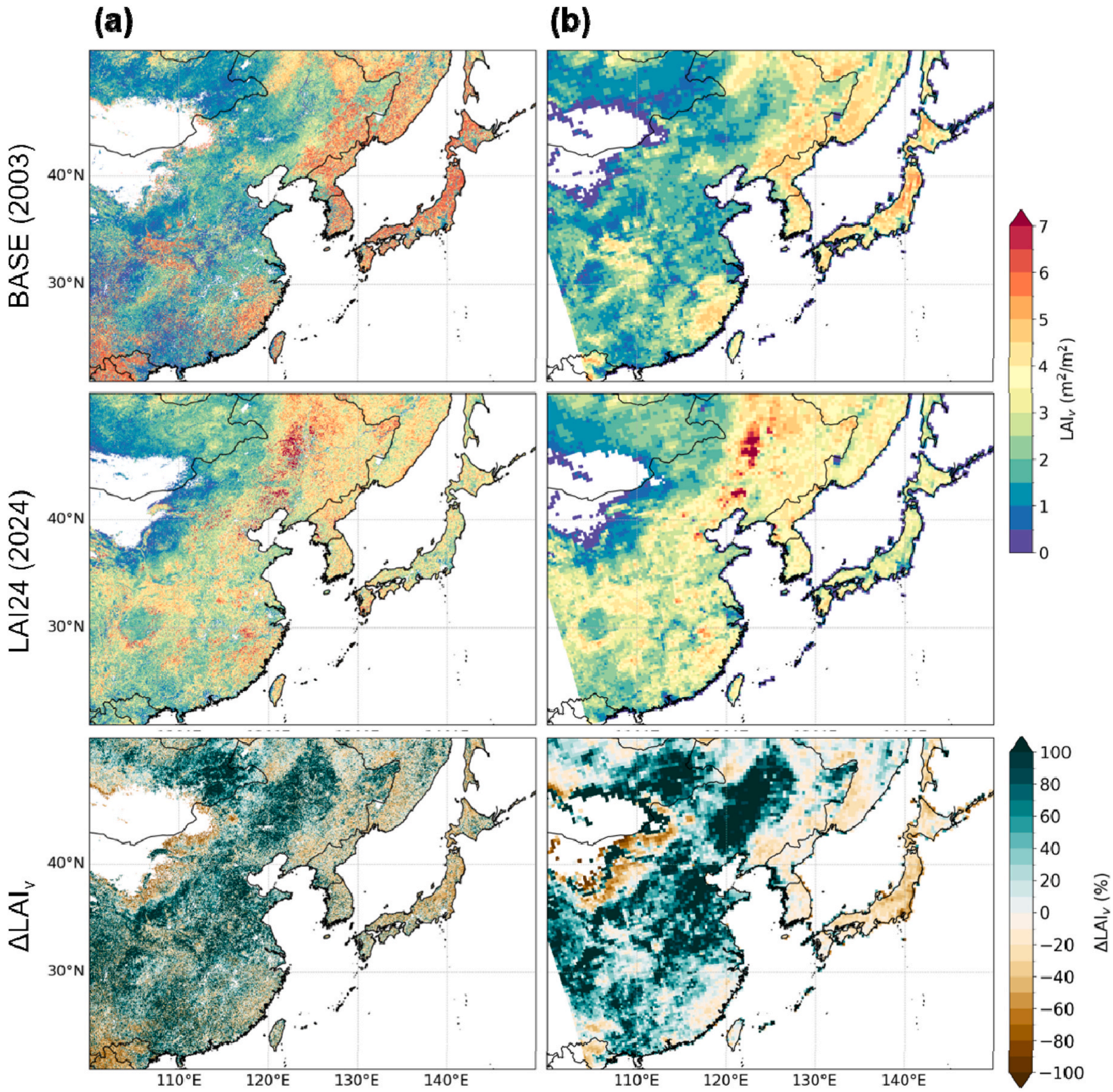

Fig. 2. Spatial distributions of LAI_v (a) from MODIS (~500 m resolution) and (b) from WRF-Chem/MEGAN using MODIS-derived inputs (27 km resolution) for the BASE simulation (2003 LAI_v) and the LAI24 simulation (2024 LAI_v), together with their relative changes (ΔLAI_v, %). The relative change represents the percentage difference between the LAI_v fields used in the BASE and LAI24 simulations, which corresponds to the MODIS-derived LAI_v difference between 2003 and 2024.

Fig. 3 further highlights the dependence of vegetation changes on baseline conditions and regional characteristics. In both China and the Korean Peninsula, areas with relatively low BASE LAI_v (<3 m^2 m^{-2}) experienced the strongest greening, with relative increases often exceeding 100 %. This indicates that sparsely vegetated regions were particularly responsive to vegetation growth over the past two decades. In contrast, Japan generally exhibits marginal or negative changes, suggesting limited potential for further greening. Across all regions, the relative magnitude of ΔLAI_v declines with increasing BASE LAI_v, reflecting a saturation effect in densely vegetated areas. Such a pattern is consistent with previous studies showing that greening signals are most pronounced in sparsely vegetated regions (Donohue et al., 2013), whereas densely forested areas tend to exhibit weaker or even negative trends (Qiu et al., 2022).

3.2. LAI_v-driven variability in BVOC emissions

Fig. 4 quantifies how changes in LAI_v propagate to BVOC emissions in the WRF-Chem/MEGAN simulations. EBIO represents the modeled BVOC emission rate, with subscripts indicating individual compounds (API for α-pinene and ISO for isoprene), and Δ denotes the percent change between the 2003 and 2024 simulations. BVOC emissions covary with LAI_v, with both the sign and magnitude closely tracking those of ΔLAI_v (Fig. 4a). This relationship is robust across regions and compounds (ΔEBIO_API: R = 0.78–0.88; ΔEBIO_ISO: R = 0.77–0.89; Fig. S3), and the distributions broadly overlap. Moreover, |ΔEBIO| increases with $|\Delta LAI_v|$ (up to ~±100 %), indicating greater emission sensitivity in areas that experienced large fractional changes in LAI_v. The observed sensitivity of BVOC emissions to LAI_v is consistent with previous studies showing that LAI changes can substantially influence BVOC emission variability (Li et al., 2022; Wang et al., 2021).

Fig. 4b further illustrates the spatial variability in the biogenic emission response across the four subregions of East Asia. Overall, emission changes generally covary with ΔLAI_v across most regions; however, the Korean Peninsula exhibits an opposite response, showing increased API emissions despite a regional decrease in LAI_v. This pattern reflects the experimental design of the WRF-Chem/MEGAN simulations, in which all input fields—including PFTs, emission factors, and land

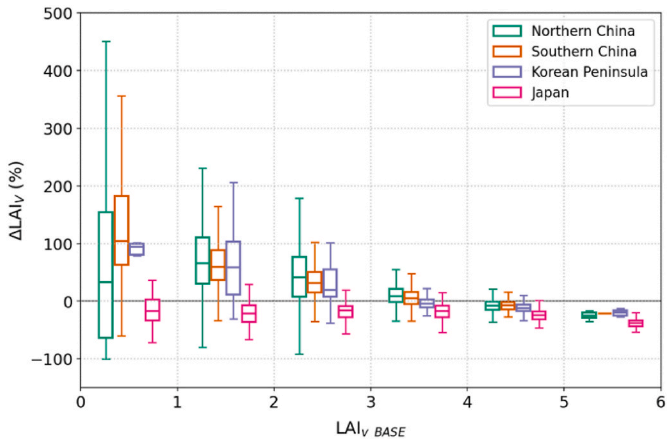

Fig. 3. ΔLAI$_v$ (%) in the LAI24 simulation (2024 LAI$_v$) relative to the BASE simulation (2003 LAI$_v$) in WRF-Chem/MEGAN, stratified by the BASE LAI$_v$ values (2003). Lower BASE LAI$_v$ values indicate sparsely vegetated conditions in 2003, whereas higher BASE LAI$_v$ values indicate densely vegetated conditions in 2003. The regions are separated into Northern China (north of 35°N), Southern China (south of 35°N), the Korean Peninsula, and Japan. All fractional changes (Δ) represent percentage differences between the BASE (2003 LAI$_v$) and LAI24 (2024 LAI$_v$) simulations.

cover—were held constant, and only LAI$_v$ was varied between the experiments. In our setup, the PFT distribution corresponds to the early-2000s vegetation dataset, when the Korean Peninsula was dominated by coniferous forests (Choung et al., 2004; Choung and Hong, 2006; Kong et al., 2014). Coniferous trees are well established as major sources of monoterpenes, particularly α-pinene, due to their high emission capacities in temperate and boreal ecosystems (Kesselmeier and Staudt, 1999; Guenther et al., 2012). Field measurements in Korea further support this, showing that *Pinus densiflora*, a representative coniferous species, emits substantial amounts of monoterpenes (Lim et al., 2008). The increase in API emissions over the Korean Peninsula therefore likely reflects the dominance of monoterpene-rich coniferous vegetation. These species exhibit a strong temperature dependence in emission rates, responding more sensitively to thermal conditions than to changes in canopy density or leaf area (Komenda and Koppmann, 2002; Schade and Goldstein, 2003; Malik et al., 2023). Consequently, even with a decline in LAI$_v$, the model simulated higher API emissions, suggesting that variations in BVOC emissions may be influenced not only by LAI$_v$ but also by the underlying species composition of the landscape.

3.3. Impacts of BVOC emission changes on air quality

Building on the finding that changes in ΔLAI$_v$ significantly affect BVOC emission fluxes (Fig. 4a), we next examined how such emission changes propagate to atmospheric pollutant concentrations (Fig. 5). The primary species considered are isoprene (ISO), α-pinene (API), limonene (LIM), and sesquiterpenes (SESQ), all of which are directly emitted BVOC species. Among them, α-pinene and limonene are classified as monoterpenes. O_3 and BSOA, which are secondarily formed via chemical pathways where these BVOCs act as key precursors, are also examined.

ΔEBIO_API exhibited strong positive correlations with monoterpene concentrations (ΔAPI and ΔLIM) and with ΔBSOA, underscoring the dominant role of monoterpenes in SOA formation. Meanwhile, ΔEBIO_ISO was tightly correlated with ΔISO and also showed strong associations with ΔSESQ, reflecting the fact that both isoprene and sesquiterpene exhibit strong temperature dependence and respond rapidly to short-term environmental variability (Sharkey and Singsaas, 1995; Duhl et al., 2008). Emission changes can co-vary when environmental forcing acts in the same direction, leading to the observed coupled responses (Hakola et al., 2003; Duhl et al., 2008). However, ΔEBIO_ISO exhibited weaker correlations with ΔBSOA, reflecting the relatively lower SOA yields of isoprene compared to monoterpenes. This finding is consistent with previous studies showing that monoterpenes are generally more efficient SOA precursors than isoprene and therefore contribute more strongly to BSOA formation (Kroll and Seinfeld, 2008; Hallquist et al., 2009; Surratt et al., 2010; Hu et al., 2013; Ehn et al., 2014; Xu et al., 2018; Xavier et al., 2019).

Correlations with ΔO_3 were weak for both ΔEBIO_API and ΔEBIO_ISO, reflecting that O_3 formation is influenced not only by BVOC emissions but also by multiple interacting factors, thereby indicating that additional processes beyond BVOC emissions govern O_3 variability (Sillman, 1999; Fiore et al., 2002; Tie et al., 2005; Cooper et al., 2014). These ΔEBIO–BVOC relationships, for the primary species (ΔISO, ΔAPI, ΔLIM, and ΔSESQ), are broadly consistent across North China, South China, the Korean Peninsula, and Japan, as shown in the region-specific ellipse plots in Fig. 5b. Region-specific correlation coefficients for both primary and secondary species further support these patterns across the four subregions (Fig. S4).

3.4. Chemical regime-dependent O_3 responses to BVOC emission changes

O_3 formation is strongly governed by the prevailing chemical regime, which differs between NO_x-limited and NO_x-saturated (VOC-limited) environments. In NO_x-saturated regimes, typically found in densely populated urban areas, O_3 production is already constrained by

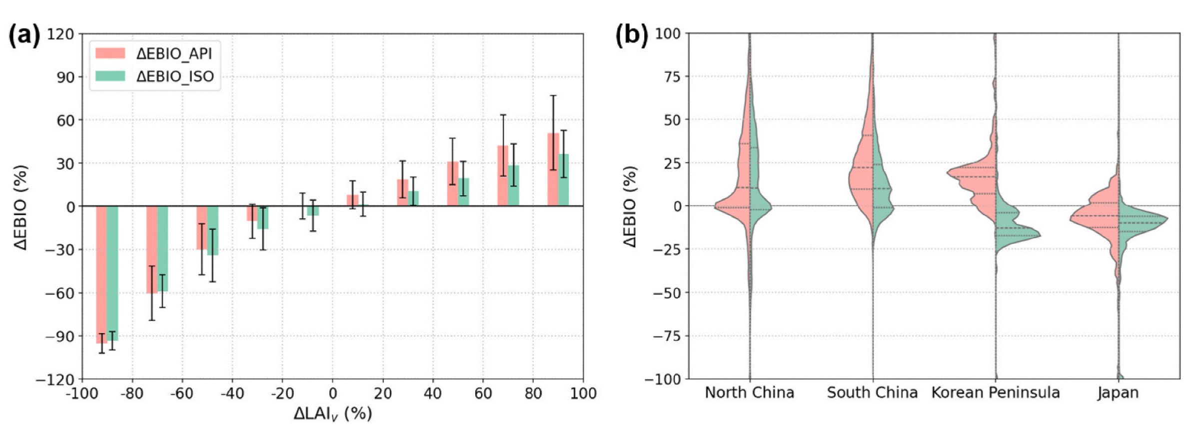

Fig. 4. Sensitivity of modeled BVOC emissions (EBIO) to changes in LAI$_v$ in WRF-Chem/MEGAN simulations. (a) Mean and standard deviation of ΔEBIO changes across ΔLAI$_v$ bins. (b) Regional distributions of ΔEBIO for Northern China, Southern China, the Korean Peninsula, and Japan. ΔEBIO includes isoprene (ΔEBIO_ISO) and α-pinene (ΔEBIO_API). Positive ΔLAI$_v$ values are associated with increased EBIO, whereas negative ΔLAI$_v$ values correspond to emission reductions.

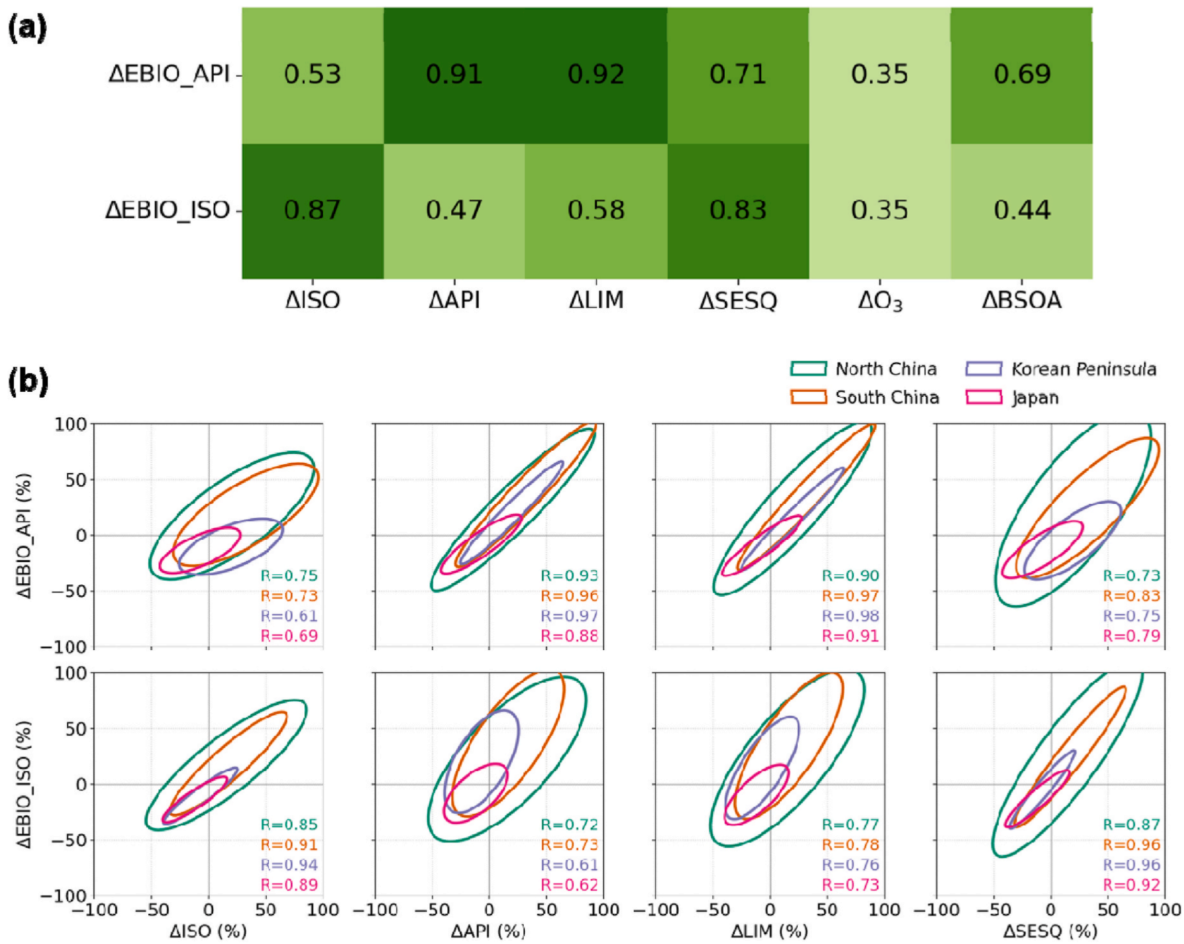

Fig. 5. Relationships between fractional changes in EBIO and atmospheric composition in WRF-Chem/MEGAN simulations. (a) Correlation coefficients (R) between ΔEBIO and changes in primary BVOC species (ΔISO, ΔAPI, ΔLIM, ΔSESQ) and secondary pollutants (ΔO_3, ΔBSOA) across East Asia. (b) Region-specific relationships between ΔEBIO and BVOC species changes for four subregions (Northern China, Southern China, the Korean Peninsula, and Japan), with ellipses indicating the 95 % confidence intervals. ΔISO, ΔAPI, ΔLIM, and ΔSESQ denote changes in isoprene, α-pinene (monoterpene), limonene (monoterpene), and sesquiterpene concentrations, respectively.

excessive NO_x levels, so additional VOC emissions tend to have limited or even suppressing effects, and effective O_3 control in such environments generally requires reductions in VOCs rather than NO_x (Sillman, 1999; Jacob, 1999; Jin and Holloway, 2015; Seinfeld and Pandis, 2016).

To examine how NO_x-saturated regimes manifest in our simulations, we analyzed changes in O_3 and BVOC emissions across representative East Asian megacities during photochemically active hours (09–18 LST) (Fig. 6). To justify the city selection, we further examined the FNR, derived from TROPOMI satellite observations for these megacities (Fig. S5). The selected cities exhibit relatively low FNR values compared to surrounding regions, consistent with NO_x-saturated conditions. Although the absolute FNR values are higher than the canonical thresholds proposed by Duncan et al. (2010), subsequent studies have shown that regime transitions often occur at higher FNR values (Jin and Holloway, 2015; Tian et al., 2025). The results show that increases in BVOC emissions were consistently accompanied by enhancements in O_3, whereas decreases in BVOC emissions were associated with reductions in O_3. This coherent covariation indicates that in NO_x-saturated environments—typical of megacities where VOCs are the limiting factor—vegetation-driven changes in BVOC emissions exert a substantial influence on urban O_3 levels. The overall pattern is robust across most regions, with China exhibiting concurrent increases and Japan showing decreases in both BVOC emissions and O_3. The Korean Peninsula, however, deviates from this relationship. This deviation may be attributed to mixed LAI_v patterns, with decreases occurring along the north–south mountain ranges in the eastern region and increases observed in several inland areas. In particular, considering the distributions of needleleaf and broadleaf trees (Fig. S6), LAI_v increases in regions dominated by needleleaf trees in South Korea contributed to increased EBIO_API, whereas LAI_v decreases in mountain regions dominated by broadleaf trees contributed to EBIO_ISO (Guenther et al., 2012; Kesselmeier and Staudt, 1999). As a result, BVOC emission changes over the Korean Peninsula exhibit bidirectional signals, as shown in Fig. 4b. These region-specific changes in BVOC emissions also influenced HO_x ($OH + HO_2$) concentrations. Fig. S7 shows the daytime and nighttime HO_x differences. Enhanced BVOC emissions associated with LAI_v increases can strengthen VOC oxidation and thereby modify HO_x production and recycling, leading to changes in HO_x levels. In China, both ΔEBIO_API and ΔEBIO_ISO increase, leading to an increase in HO_x concentrations, whereas Japan shows the opposite behavior. Over the Korean Peninsula, however, HO_x decreases during the daytime but increases at night. This contrasting behavior likely reflects the different dominant oxidation pathways of API and ISO across the diurnal cycle: API is oxidized more efficiently at night via NO_3^- radical chemistry, whereas ISO undergoes active oxidation by OH during the daytime, exerting a strong influence on the daytime HO_x budget under photochemical conditions. Accordingly, the daytime reduction in HO_x over the Korean Peninsula is interpreted to be associated with decreased ΔEBIO_ISO, while the nighttime enhancement in HO_x is linked to increased ΔEBIO_API. Overall, the opposing contributions of ΔEBIO_API

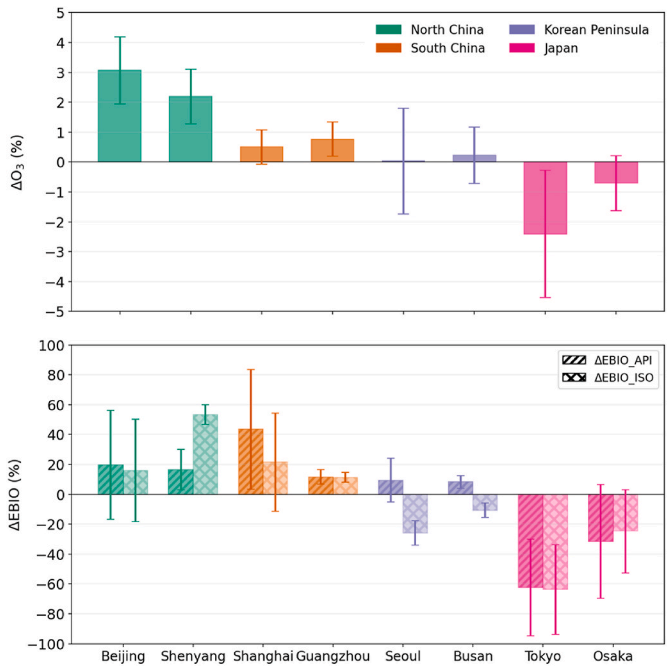

Fig. 6. Changes in O_3 and EBIO across representative East Asian megacities during photochemically active hours (09–18 LST). Bars represent mean percentage changes in the LAI24 (2024 LAI_v) simulation relative to the BASE (2003 LAI_v) simulation, and error bars denote standard deviations. Across most cities, O_3 changes are consistent with EBIO changes.

and ΔEBIO_ISO, together with the resulting day–night differences in radical responses and regional heterogeneity in trends, produce substantial compensation effects. Consequently, the domain-averaged ΔO_3 over the Korean Peninsula shows little overall change.

To further investigate the spatial heterogeneity of these responses, we analyzed ΔO_3, ΔEBIO, and ΔLAI_v as a function of the FNR-based chemical regime classification, using WRF-Chem simulations collocated with TROPOMI retrievals (Fig. 7). The largest increases in ΔO_3 were observed at intermediate FNR values of 3–6. In these regions, ΔLAI_v showed the strongest positive changes, which translated into substantial increases in ΔEBIO. At the same time, ambient NO_2 levels remained sufficiently high to sustain efficient O_3 production. This combination of enhanced biogenic precursors and adequate NO_x availability created conditions that maximize photochemical O_3 formation. By contrast, in areas with low FNR values, corresponding to NO_x-saturated urban cores, LAI_v changes and associated BVOC responses were relatively small, resulting in weaker O_3 signals. Conversely, at high FNR values, characteristic of NO_x-limited background regions, O_3 responses were muted due to insufficient NO_x despite notable BVOC increases. Overall, these results highlight suburban transition zones with intermediate FNR values (around 3–6) as the regions where vegetation-driven changes exert the strongest influence on O_3.

3.5. Urban–suburban contrasts in BSOA responses to BVOC emission changes

BSOA responses were analyzed with a focus on α-pinene (API) emissions, which exhibited stronger correlations with BSOA than isoprene emissions as discussed in Section 3.3. Fig. 8a presents the spatial distributions of NO_2, ΔEBIO_API, and ΔBSOA across East Asia.

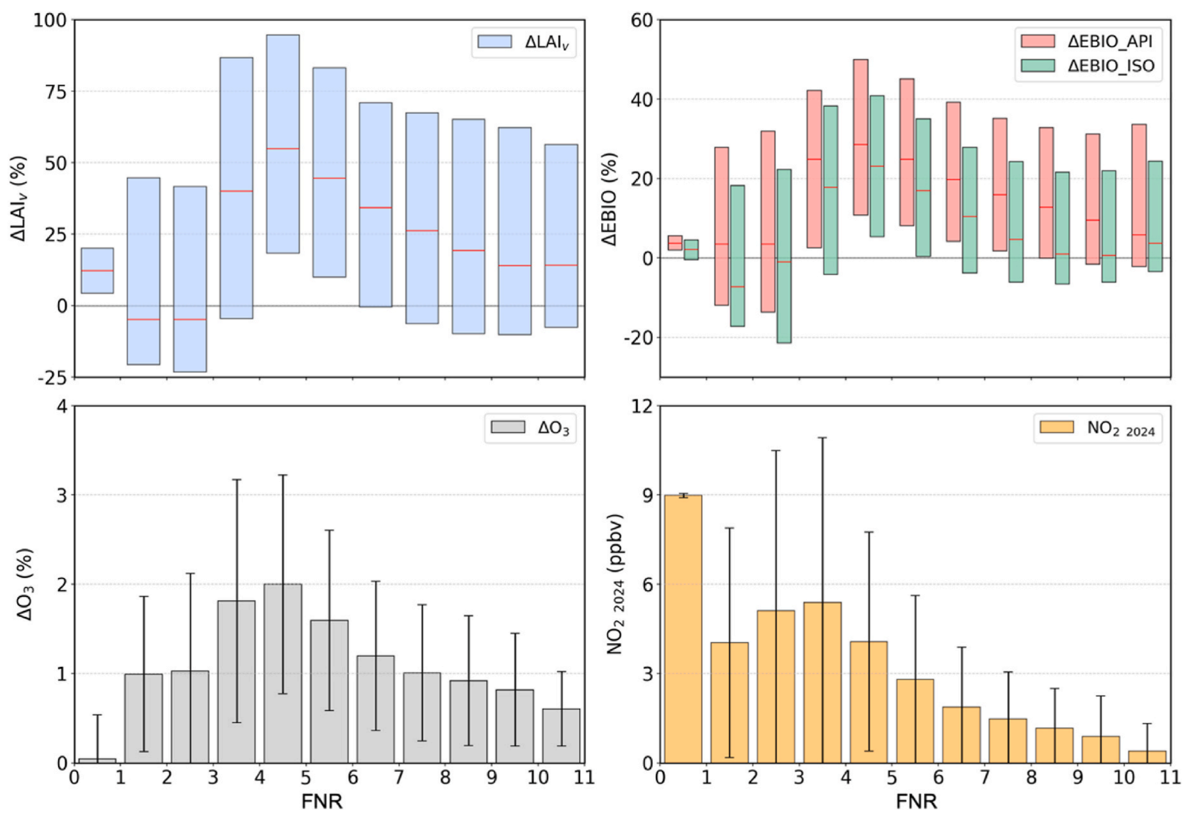

Fig. 7. Responses of ΔLAI_v, ΔEBIO, and ΔO_3, along with NO_2 concentrations, as a function of the formaldehyde-to-nitrogen dioxide ratio (FNR = $HCHO/NO_2$) derived from TROPOMI observations. Panels show ΔLAI_v, ΔEBIO, ΔO_3, and NO_2 concentrations from WRF-Chem simulations. ΔLAI_v, ΔEBIO, and ΔO_3 represent percentage changes in the LAI24 (2024 LAI_v) simulation relative to the BASE (2003 LAI_v) simulation, whereas NO_2 denotes the concentration in the LAI24 simulation. Values are summarized across FNR bins to illustrate how LAI_v-driven EBIO changes and O_3 responses vary across photochemical regimes, with NO_2 included to indicate concentration levels associated with each FNR bin.

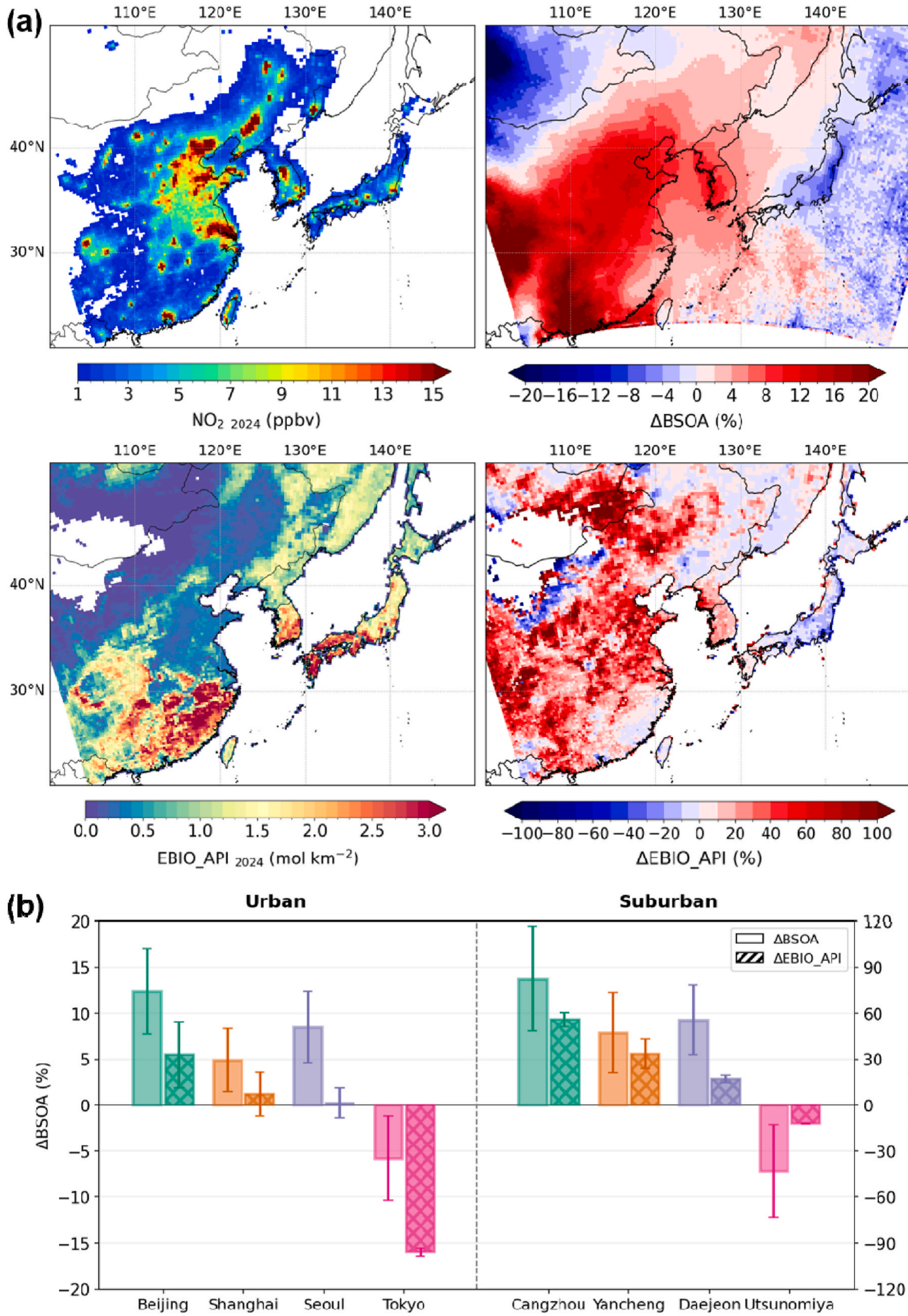

Fig. 8. (a) Spatial distributions of modeled NO_2 concentrations in the LAI24 (2024 LAI_v) simulation, EBIO_API in the LAI24 simulation, and their fractional changes (ΔEBIO_API, %) together with ΔBSOA (%) from WRF-Chem/MEGAN simulations. ΔEBIO_API and ΔBSOA represent percentage changes in the LAI24 simulation relative to the BASE (2003 LAI_v) simulation. (b) Comparison of urban and suburban responses in ΔBSOA (%) and ΔEBIO_API (%) for representative megacities in China, Korea, and Japan.

The maps reveal broadly consistent spatial patterns between ΔEBIO_API and ΔBSOA. In particular, large positive ΔBSOA values appear over China and parts of the Korean Peninsula, where ΔEBIO_API is also elevated, suggesting that LAI_v-driven increases in monoterpene fluxes contributed to greater BSOA formation. Conversely, Japan shows smaller or negative changes in both ΔEBIO_API and ΔBSOA, reflecting reduced biogenic precursor availability.

Fig. 8b provides a more detailed comparison between urban and suburban regions, highlighting regional contrasts in ΔBSOA and ΔEBIO_API responses. Based on the NO_2 distributions in Fig. 8a, urban and suburban regions were delineated to assess how BSOA responses differ under varying NO_x environments. In China and the Korean Peninsula, both ΔBSOA and ΔEBIO_API exhibit positive changes, with suburban sites (Cangzhou, Yancheng, Daejeon) showing larger increases than their urban counterparts (Beijing, Shanghai, Seoul). This pattern suggests that BSOA formation is more efficient in suburban regions with moderate NO_x levels than in highly NO_x-saturated urban areas, consistent with chamber and field studies showing that excessive NO_x suppresses SOA yields (Presto et al., 2005; Ng et al., 2007; Donahue et al., 2014). The stronger BSOA response in suburban regions likely reflects the combined effects of greater vegetation increases (larger ΔLAI_v; Fig. 7) and more favorable NO_x conditions for SOA formation.

In contrast, Japan shows overall decreases in both ΔBSOA and ΔEBIO_API, consistent with the regional decline in ΔLAI_v. The reductions are most pronounced over urban areas such as Tokyo, where NO_x-saturated conditions suppress SOA formation efficiency and amplify the impact of declining monoterpene emissions. As a result, BSOA decreases more sharply in urban regions, where excessive NO_x inhibits efficient oxidation of monoterpenes, whereas suburban areas with moderate NO_x levels sustain more favorable conditions for SOA formation. These results indicate that under declining vegetation activity, BSOA formation in Japan is primarily constrained by the chemical environment rather than by emission magnitude alone.

4. Conclusions

This study investigated the influence of vegetation structural changes on BVOC emissions and regional air quality over East Asia using the WRF-Chem/MEGAN simulations constrained by MODIS-derived LAI_v fields for 2003 and 2024. The results reveal an overall greening trend across East Asia, but with distinct regional contrasts: substantial increases occurred over China and parts of the Korean Peninsula, whereas Japan exhibited localized declines associated with vegetation loss. BVOC emissions were found to covary strongly with changes in LAI_v, emphasizing the dominant role of vegetation activity in controlling emission fluxes.

The resulting impacts on secondary pollutants were, however, jointly regulated by vegetation changes and the prevailing chemical regime. Suburban regions, which experienced larger increases in LAI_v than urban cores, showed stronger enhancements in BVOC emissions and more pronounced O_3 responses, amplified under moderate NO_x conditions that favor efficient photochemical oxidation. In contrast, NO_x-saturated urban environments exhibited weaker O_3 changes because excessive NO_x suppressed the photochemical efficiency of VOC oxidation, limiting O_3 formation despite active photochemical conditions.

Among the BVOC species, monoterpenes—particularly α-pinene—exhibited a much stronger association with BSOA formation than isoprene, consistent with their substantially higher SOA yields. Spatially, regions with enhanced monoterpene emissions also showed pronounced increases in BSOA, underscoring the key role of monoterpenes as major precursors of organic aerosol formation. The stronger BSOA responses observed in suburban regions can be attributed to the combined effects of greater vegetation increases and more favorable NO_x conditions for oxidation, whereas highly NO_x-saturated urban areas exhibited weaker or even negative responses.

Overall, this work highlights that vegetation dynamics and chemical environments jointly regulate BVOC–SOA–O_3 interactions across East Asia. As vegetation continues to evolve under changing climate and land-use conditions, understanding these coupled biogenic–atmospheric feedbacks will be critical for predicting future air quality and radiative forcing in the region.

While the present study focuses on the sensitivity of BVOC emissions to vegetation structural changes represented by LAI_v, some uncertainties remain. The MEGAN framework includes uncertainties associated with emission factors, PFT distributions, and activity algorithms (Guenther et al., 2012; Sindelarova et al., 2014). However, the same model configuration and emission factors were applied consistently in both simulations; therefore, the relative differences reported here primarily reflect the impact of LAI_v changes rather than uncertainties in model parameters. In addition, the analysis focuses on August 2024, which represents a period of strong vegetation activity and relatively weak monsoon influence during the simulated summer season. Although BVOC emissions and their atmospheric impacts may vary under different meteorological conditions and in other seasons, the present results provide process-level insight into LAI_v–BVOC–air-quality interactions under peak biogenic emission conditions. Future studies incorporating multi-seasonal or multi-year simulations, as well as land-cover changes, would enable a more comprehensive assessment of vegetation-driven BVOC emissions and their implications for regional air quality.

CRediT authorship contribution statement

Seung-Hee Baek: Writing – review & editing, Writing – original draft, Visualization, Conceptualization. **Hyo-Jung Lee:** Writing – review & editing, Writing – original draft, Visualization, Supervision, Investigation, Conceptualization. **Yu-Jin Jo:** Writing – review & editing, Writing – original draft, Supervision, Conceptualization. **Younha Kim:** Writing – review & editing, Methodology, Investigation. **Min-Jun Park:** Writing – review & editing, Visualization, Investigation. **Cheol-Hee Kim:** Writing – review & editing, Investigation.

Funding sources

This work was supported by the Basic Science Research Program through the National Research Foundation of Korea (NRF), funded by the Ministry of Education [RS-2020-NR049592] to Seung-Hee Baek, Hyo-Jung Lee, Yu-Jin Jo, Min-Jun Park, and Cheol-Hee Kim; and by the NRF [RS-2022-NR069425], funded by the Korean Government (MSIT) to Seung-Hee Baek, Hyo-Jung Lee, and Min-Jun Park.

Declaration of competing interest

The authors declare that they have no known competing financial interests or personal relationships that could have appeared to influence the work reported in this paper.

Acknowledgements

We gratefully acknowledge the TROPOMI team for providing the NO_2 and HCHO data and the MODIS team for providing the Leaf Area Index (LAI) and Vegetation Continuous Fields (VCF) products used in this study.

Appendix A. Supplementary data

Supplementary data to this article can be found online at https://doi.org/10.1016/j.envres.2026.124392.

Data availability

Data will be made available on request.

References

Ackermann, I.J., Hass, H., Memmesheimer, M., Ebel, A., Binkowski, F.S., Shankar, U., 1998. Modal aerosol dynamics model for Europe: development and first applications. Atmos. Environ. 32, 2981–2999. https://doi.org/10.1016/S1352-2310(98)00006-5.

Ahmadov, R., McKeen, S.A., Robinson, A.L., Bahreini, R., Middlebrook, A.M., de Gouw, J.A., Meagher, J., Hsie, E.-Y., Edgerton, E., Shaw, S., Trainer, M., 2012. A volatility basis set model for summertime secondary organic aerosols over the eastern United States in 2006. J. Geophys. Res. 117, D06301. https://doi.org/10.1029/2011JD016831.

Atkinson, R., Arey, J., 2003. Gas-phase tropospheric chemistry of biogenic volatile organic compounds: a review. Atmos. Environ. 37, 197–219. https://doi.org/10.1016/S1352-2310(03)00391-1.

Bash, J.O., Baker, K.R., Beaver, M.R., 2016. Evaluation of improved land use and canopy representation in BEIS v3.61 with biogenic VOC measurements in California. Geosci. Model Dev. (GMD) 9, 2191–2207. https://doi.org/10.5194/gmd-9-2191-2016.

Carlton, A.G., Wiedinmyer, C., Kroll, J.H., 2009. A review of secondary organic aerosol (SOA) formation from isoprene. Atmos. Chem. Phys. 9, 4987–5005. https://doi.org/10.5194/acp-9-4987-2009.

Chen, C., Park, T., Wang, X., Piao, S., Xu, B., Chaturvedi, R.K., Fuchs, R., Brovkin, V., Ciais, P., Fensholt, R., Tømmervik, H., Bala, G., Zhu, Z., Nemani, R.R., Myneni, R.B., 2019. China and India lead in greening of the world through land-use management. Nat. Sustain. 2, 122–129. https://doi.org/10.1038/s41893-019-0220-7.

Chen, X., Chen, T., He, B., Liu, S., Zhou, S., Shi, T., 2024. The global greening continues despite increased drought stress since 2000. Glob. Ecol. Conserv. 49, e02791. https://doi.org/10.1016/j.gecco.2023.e02791.

Chen, Y., Chen, L., Cheng, Y., Ju, W., Chen, H.Y.H., Ruan, H., 2020. Afforestation promotes the enhancement of forest LAI and NPP in China. For. Ecol. Manag. 462, 117990. https://doi.org/10.1016/j.foreco.2020.117990.

Cheng, S., Guan, X., Huang, J., Ji, F., Guo, R., 2015. Long-term trend and variability of soil moisture over East Asia. JGR Atmospheres 120, 8658–8670. https://doi.org/10.1002/2015JD023206.

Choung, H.-L., Hong, S.-K., 2006. Distribution patterns, floristic differentiation and succession of Pinus densiflora forest in South Korea: a perspective at nation-wide scale. Phytocoenologia 36, 213–229. https://doi.org/10.1127/0340-269X/2006/0036-0213.

Choung, Y., Lee, B.-C., Cho, J.-H., Lee, K.-S., Jang, I.-S., Kim, S.-H., Hong, S.-K., Jung, H.-C., Choung, H.-L., 2004. Forest responses to the large-scale east coast fires in Korea. Ecol. Res. 19, 43–54. https://doi.org/10.1111/j.1440-1703.2003.00607.x.

Cooper, O.R., Parrish, D.D., Ziemke, J., Balashov, N.V., Cupeiro, M., Galbally, I.E., Gilge, S., Horowitz, L., Jensen, N.R., Lamarque, J.-F., Naik, V., Oltmans, S.J., Schwab, J., Shindell, D.T., Thompson, A.M., Thouret, V., Wang, Y., Zbinden, R.M., 2014. Global distribution and trends of tropospheric ozone: an observation-based review. Elem. Sci. Anth 2. https://doi.org/10.12952/journal.elementa.000029.

Donahue, N.M., Robinson, A.L., Trump, E.R., Riipinen, I., Kroll, J.H., 2014. Volatility and aging of atmospheric organic aerosol. Top. Curr. Chem. 339, 97–143. https://doi.org/10.1007/128_2012_355.

Donohue, R.J., Roderick, M.L., McVicar, T.R., Farquhar, G.D., 2013. Impact of CO_2 fertilization on maximum foliage cover across the globe's warm, arid environments. Geophys. Res. Lett. 40, 3031–3035. https://doi.org/10.1002/grl.50563.

Duan, C., Liao, H., Wang, K., Ren, Y., 2023. The research hotspots and trends of volatile organic compound emissions from anthropogenic and natural sources: a systematic quantitative review. Environ. Res. 216, 114386. https://doi.org/10.1016/j.envres.2022.114386.

Duhl, T.R., Helmig, D., Guenther, A., 2008. Sesquiterpene emissions from vegetation: a review. Biogeosciences 5, 761–777. https://doi.org/10.5194/bg-5-761-2008.

Duncan, B.N., Yoshida, Y., Olson, J.R., Sillman, S., Martin, R.V., Lamsal, L., Hu, Y., Pickering, K.E., Retscher, C., Allen, D.J., Crawford, J.H., 2010. Application of OMI observations to a space-based indicator of NO_x and VOC controls on surface ozone formation. Atmos. Environ. 44, 2213–2223. https://doi.org/10.1016/j.atmosenv.2010.03.010.

Ehn, M., Thornton, J.A., Kleist, E., Sipilä, M., Junninen, H., Pullinen, I., Springer, M., Rubach, F., Tillmann, R., Lee, B., Lopez-Hilfiker, F., Andres, S., Acir, I.-H., Rissanen, M., Jokinen, T., Schobesberger, S., Kangasluoma, J., Kontkanen, J., Nieminen, T., Kurtén, T., Nielsen, L.B., Jørgensen, S., Kjaergaard, H.G., Canagaratna, M., Maso, M.D., Berndt, T., Petäjä, T., Wahner, A., Kerminen, V.-M., Kulmala, M., Worsnop, D.R., Wildt, J., Mentel, T.F., 2014. A large source of low-volatility secondary organic aerosol. Nature 506, 476–479. https://doi.org/10.1038/nature13032.

Fang, H., Baret, F., Plummer, S., Schaepman-Strub, G., 2019. An overview of global leaf Area index (LAI): methods, products, validation, and applications. Rev. Geophys. 57, 739–799. https://doi.org/10.1029/2018RG000608.

Fiore, A.M., Jacob, D.J., Field, B.D., Streets, D.G., Fernandes, S.D., Jang, C., 2002. Linking ozone pollution and climate change: the case for controlling methane. Geophys. Res. Lett. 29, 1919. https://doi.org/10.1029/2002GL015601.

Fiore, A.M., Naik, V., Spracklen, D.V., Steiner, A., Unger, N., Prather, M., Bergmann, D., Cameron-Smith, P.J., Cionni, I., Collins, W.J., Dalsøren, S., Eyring, V., Folberth, G.A., Ginoux, P., Horowitz, L.W., Josse, B., Lamarque, J.-F., MacKenzie, I.A., Nagashima, T., O'Connor, F.M., Righi, M., Rumbold, S.T., Shindell, D.T., Skeie, R.B., Sudo, K., Szopa, S., Takemura, T., Zeng, G., 2012. Global air quality and climate. Chem. Soc. Rev. 41, 6663–6683. https://doi.org/10.1039/c2cs35095e.

Gai, Y., Sun, L., Fu, S., Zhu, C., Zhu, C., Li, R., Liu, Z., Wang, B., Wang, C., Yang, N., Li, J., Xu, C., Yan, G., 2024. Impact of greening trends on biogenic volatile organic compound emissions in China from 1985 to 2022: contributions of afforestation projects. Sci. Total Environ. 929, 172551. https://doi.org/10.1016/j.scitotenv.2024.172551.

Gao, M., Wang, X., Meng, F., Liu, Q., Li, X., Zhang, Y., Piao, S., 2020. Three-dimensional change in temperature sensitivity of northern vegetation phenology. Glob. Change Biol. 26, 5189–5201. https://doi.org/10.1111/gcb.15200.

GCOS, 2011. Systematic observation requirements for satellite-based products for climate. Update, GCOS-154. World Meteorological Organization, Geneva, Switzerland. https://ceos.org/document_management/Working_Groups/WGClimate/Documents/gcos-154.pdf.

Grell, G.A., Peckham, S.E., Schmitz, R., McKeen, S.A., Frost, G., Skamarock, W.C., Eder, B., 2005. Fully coupled "online" chemistry within the WRF model. Atmos. Environ. 39, 6957–6975. https://doi.org/10.1016/j.atmosenv.2005.04.027.

Gu, D., Guenther, A.B., Shilling, J.E., Yu, H., Huang, M., Zhao, C., Yang, Q., Martin, S.T., Artaxo, P., Kim, S., Seco, R., Stavrakou, T., Longo, K.M., Tóta, J., de Souza, R.A.F., Vega, O., Liu, Y., Shrivastava, M., Alves, E.G., Santos, F.C., Leng, G., Hu, Z., 2017. Airborne observations reveal elevational gradient in tropical forest isoprene emissions. Nat. Commun. 8, 15541. https://doi.org/10.1038/ncomms15541.

Guenther, A., Karl, T., Harley, P., Wiedinmyer, C., Palmer, P.I., Geron, C., 2006. Estimates of global terrestrial isoprene emissions using MEGAN (Model of emissions of gases and aerosols from nature). Atmos. Chem. Phys. 6, 3181–3210. https://doi.org/10.5194/acp-6-3181-2006.

Guenther, A.B., Jiang, X., Heald, C.L., Sakulyanontvittaya, T., Duhl, T., Emmons, L.K., Wang, X., 2012. The model of emissions of gases and aerosols from nature version 2.1 (MEGAN2.1): an extended and updated framework for modeling biogenic emissions. Geosci. Model Dev. (GMD) 5, 1471–1492. https://doi.org/10.5194/gmd-5-1471-2012.

Hakola, H., Tarvainen, V., Laurila, T., Hiltunen, V., Hellén, H., Keronen, P., 2003. Seasonal variation of VOC concentrations above a boreal coniferous forest. Atmos. Environ. 37, 1623–1634. https://doi.org/10.1016/S1352-2310(03)00014-1.

Hallquist, M., Wenger, J.C., Baltensperger, U., Rudich, Y., Simpson, D., Claeys, M., Dommen, J., Donahue, N.M., George, C., Goldstein, A.H., Hamilton, J.F., Herrmann, H., Hoffmann, T., Iinuma, Y., Jang, M., Jenkin, M.E., Jimenez, J.L., Kiendler-Scharr, A., Maenhaut, W., McFiggans, G., Mentel, T.F., Monod, A., Prévôt, A.S.H., Seinfeld, J.H., Surratt, J.D., Szmigielski, R., Wildt, J., 2009. The formation, properties and impact of secondary organic aerosol: current and emerging issues. Atmos. Chem. Phys. 9, 5155–5236. https://doi.org/10.5194/acp-9-5155-2009.

Han, G., Wang, J., Pan, Y., Huang, N., Zhang, Z., Peng, R., Wang, Z., Sun, G., Liu, C., Ma, S., Song, Y., Pan, Z., 2020. Temporal and spatial variation of soil moisture and its possible impact on regional air temperature in China. Water 12, 1807. https://doi.org/10.3390/w12061807.

Hansen, M.C., DeFries, R.S., Townshend, J.R.G., Carroll, M., Dimiceli, C., Sohlberg, R.A., 2003. Global percent tree cover at a spatial resolution of 500 meters: first results of the MODIS vegetation continuous fields algorithm. Earth Interact. 7, 1–15. https://doi.org/10.1175/1087-3562(2003)007<0001:GPTCAA>2.0.CO, 2.

Hu, Q.-H., Xie, Z.-Q., Wang, X.-M., Kang, H., He, Q.-F., Zhang, P., 2013. Secondary organic aerosols over oceans via oxidation of isoprene and monoterpenes from arctic to antarctic. Sci. Rep. 3, 2280. https://doi.org/10.1038/srep02280.

Jacob, D.J., 1999. Introduction to Atmospheric Chemistry. Princeton University Press, Princeton, New Jersey. https://doi.org/10.2307/j.ctt7t8hg.

Jin, X., Holloway, T., 2015. Spatial and temporal variability of ozone sensitivity over China observed from the ozone monitoring instrument. JGR Atmospheres 120, 7229–7246. https://doi.org/10.1002/2015JD023250.

Jin, Z., You, Q., Zuo, Z., Li, M., Sun, G., Pepin, N., Wang, L., 2023. Increased sensitivity of greening to afforestation in China over the recent 20 years. Agric. For. Meteorol. 339, 109561. https://doi.org/10.1016/j.agrformet.2023.109561.

Kesselmeier, J., Staudt, M., 1999. Biogenic volatile organic compounds (VOC): an overview on emission, physiology and ecology. J. Atmos. Chem. 33, 23–88. https://doi.org/10.1023/A:1006127516791.

Kim, S., Kim, J., Hu, H., Jang, M., Lee, J.-B., Hong, S.C., Kim, O., Woo, J.-H., 2023. Update of the year 2019 modeling emission inventory in China. Asian J. Atmos. Environ. 17, 20. https://doi.org/10.1007/s44273-023-00012-x.

Komenda, M., Koppmann, R., 2002. Monoterpene emissions from Scots pine (Pinus sylvestris): field studies of emission rate variabilities. J. Geophys. Res. 107, 1. https://doi.org/10.1029/2001JD000691.

Kong, W.-S., Lee, S.-G., Park, H.-N., Lee, Y.-M., Oh, S.-H., 2014. Time-spatial distribution of Pinus in the Korean Peninsula. Quat. Int. 344, 43–52. https://doi.org/10.1016/j.quaint.2014.03.038.

Kroll, J.H., Seinfeld, J.H., 2008. Chemistry of secondary organic aerosol: formation and evolution of low-volatility organics in the atmosphere. Atmos. Environ. 42, 3593–3624. https://doi.org/10.1016/j.atmosenv.2008.01.003.

Li, J., Han, Z., Wu, J., Wang, Q., Li, J., Tao, J., 2022. Changes in summer biogenic volatile organic compound emission and secondary organic aerosols over the 2001–2018 period over China: roles of leaf biomass, meteorology, and anthropogenic emission variability. Atmos. Res. 280, 106450. https://doi.org/10.1016/j.atmosres.2022.106450.

Lim, J.-H., Kim, J.-C., Kim, K.-J., Son, Y.-S., Sunwoo, Y., Han, J.-S., 2008. Seasonal variations of monoterpene emissions from Pinus densiflora in East Asia. Chemosphere 73, 470–478. https://doi.org/10.1016/j.chemosphere.2008.06.048.

Liu, S., Xing, J., Zhang, H., Ding, D., Zhang, F., Zhao, B., Sahu, S.K., Wang, S., 2019. Climate-driven trends of biogenic volatile organic compound emissions and their impacts on summertime ozone and secondary organic aerosol in China in the 2050s. Atmos. Environ. 218, 117020. https://doi.org/10.1016/j.atmosenv.2019.117020.

Liu, Y., Chen, T., Ma, Z., Li, Q., Gao, Y., Xue, L., Wang, W., 2025. Variation of biogenic VOC contribution to ozone formation with reduced anthropogenic precursor emissions: coupling online observation and future scenario simulation. Sci. Total Environ. 961, 178380. https://doi.org/10.1016/j.scitotenv.2025.178380.

Lorente, A., Borsdorff, T., Butz, A., Hasekamp, O., aan de Brugh, J., Schneider, A., Wu, L., Hase, F., Kivi, R., Wunch, D., Pollard, D.F., Shiomi, K., Deutscher, N.M., Velazco, V. A., Roehl, C.M., Wennberg, P.O., Warneke, T., Landgraf, J., 2021. Methane retrieved from TROPOMI: improvement of the data product and validation of the first 2 years of measurements. Atmos. Meas. Tech. 14, 665–684. https://doi.org/10.5194/amt-14-665-2021.

Lou, C., Jiang, F., Tian, X., Zou, Q., Zheng, Y., Shen, Y., Feng, S., Chen, J., Zhang, L., Jia, M., Xu, J., 2023. Modeling the biogenic isoprene emission and its impact on ozone pollution in Zhejiang Province, China. Sci. Total Environ. 865, 161212. https://doi.org/10.1016/j.scitotenv.2022.161212.

Lyu, X., Li, H., Lee, S.-C., Xiong, E., Guo, H., Wang, T., de Gouw, J., 2024. Significant biogenic source of oxygenated volatile organic compounds and the impacts on photochemistry at a regional background site in South China. Environ. Sci. Technol. 58, 20081–20090. https://doi.org/10.1021/acs.est.4c05656.

Malik, T.G., Sahu, L.K., Gupta, M., Mir, B.A., Gajbhiye, T., Dubey, R., Clavijo McCormick, A., Pandey, S.K., 2023. Environmental factors affecting monoterpene emissions from terrestrial vegetation. Plants 12, 3146. https://doi.org/10.3390/plants12173146.

Myneni, R.B., Hoffman, S., Knyazikhin, Y., Privette, J.L., Glassy, J., Tian, Y., Wang, Y., Song, X., Zhang, Y., Smith, G.R., Lotsch, A., Friedl, M., Morisette, J.T., Votava, P., Nemani, R.R., Running, S.W., 2002. Global products of vegetation leaf area and fraction absorbed PAR from year one of MODIS data. Remote Sens. Environ. 83, 214–231. https://doi.org/10.1016/S0034-4257(02)00074-3.

Myneni, R.B., Keeling, C.D., Tucker, C.J., Asrar, G., Nemani, R.R., 1997. Increased plant growth in the northern high latitudes from 1981 to 1991. Nature 386, 698–702. https://doi.org/10.1038/386698a0.

NCEP, U.S.D. of C, 2015. NCEP GDAS/FNL 0.25 degree global tropospheric analyses and forecast grids. https://doi.org/10.5065/D65Q4T4Z.

Ng, N.L., Chhabra, P.S., Chan, A.W.H., Surratt, J.D., Kroll, J.H., Kwan, A.J., McCabe, D. C., Wennberg, P.O., Sorooshian, A., Murphy, S.M., Dalleska, N.F., Flagan, R.C., Seinfeld, J.H., 2007. Effect of NO_x level on secondary organic aerosol (SOA) formation from the photooxidation of terpenes. Atmos. Chem. Phys. 7, 5159–5174. https://doi.org/10.5194/acp-7-5159-2007.

Piao, S., Liu, Q., Chen, A., Janssens, I.A., Fu, Y., Dai, J., Liu, L., Lian, X., Shen, M., Zhu, X., 2019. Plant phenology and global climate change: current progresses and challenges. Glob. Change Biol. 25, 1922–1940. https://doi.org/10.1111/gcb.14619.

Piao, S., Wang, X., Park, T., Chen, C., Lian, X., He, Y., Bjerke, J.W., Chen, A., Ciais, P., Tømmervik, H., Nemani, R.R., Myneni, R.B., 2020. Characteristics, drivers and feedbacks of global greening. Nat. Rev. Earth Environ. 1, 14–27. https://doi.org/10.1038/s43017-019-0001-x.

Piao, S., Yin, G., Tan, J., Cheng, L., Huang, M., Li, Y., Liu, R., Mao, J., Myneni, R.B., Peng, S., Poulter, B., Shi, X., Xiao, Z., Zeng, N., Zeng, Z., Wang, Y., 2015. Detection and attribution of vegetation greening trend in China over the last 30 years. Glob. Change Biol. 21, 1601–1609. https://doi.org/10.1111/gcb.12795.

Pierce, T.E., Waldruff, P.S., 1991. PC-BEIS: a personal computer version of the biogenic emissions inventory system. J. Air Waste Manag. Assoc. 41, 937–941. https://doi.org/10.1080/10473289.1991.10466890.

Presto, A.A., Hartz, K.E.H., Donahue, N.M., 2005. Secondary organic aerosol production from terpene ozonolysis. 2. Effect of NO_x concentration. Environ. Sci. Technol. 39, 7046–7054. https://doi.org/10.1021/es050400s.

Pullinen, I., Schmitt, S., Kang, S., Sarrafzadeh, M., Schlag, P., Andres, S., Kleist, E., Mentel, T.F., Rohrer, F., Springer, M., Tillmann, R., Wildt, J., Wu, C., Zhao, D., Wahner, A., Kiendler-Scharr, A., 2020. Impact of NO_x on secondary organic aerosol (SOA) formation from α-pinene and β-pinene photooxidation: the role of highly oxygenated organic nitrates. Atmos. Chem. Phys. 20, 10125–10147. https://doi.org/10.5194/acp-20-10125-2020.

Qiu, B., Ye, Z., Chen, C., Tang, Z., Chen, Z., Huang, H., Zhao, Z., Xu, W., Berry, J., 2022. Dense canopies browning overshadowed by global greening dominant in sparse canopies. Sci. Total Environ. 826, 154222. https://doi.org/10.1016/j.scitotenv.2022.154222.

Schade, G.W., Goldstein, A.H., 2003. Increase of monoterpene emissions from a pine plantation as a result of mechanical disturbances. Geophys. Res. Lett. 30, 1380. https://doi.org/10.1029/2002GL016138.

Seinfeld, J.H., Pandis, S.N., 2016. Atmos. Chem. Phys.: from Air Pollution to Climate Change, second ed. John Wiley & Sons, New Jersey.

Sharkey, T.D., Singsaas, E.L., 1995. Why plants emit isoprene. Nature 374, 769. https://doi.org/10.1038/374769a0.

Sillman, S., 1999. The relation between ozone, NO_x and hydrocarbons in urban and polluted rural environments. Atmos. Environ. 33, 1821–1845. https://doi.org/10.1016/S1352-2310(98)00345-8.

Sindelarova, K., Granier, C., Bouarar, I., Guenther, A., Tilmes, S., Stavrakou, T., Müller, J. F., Kuhn, U., Stefani, P., Knorr, W., 2014. Global data set of biogenic VOC emissions calculated by the MEGAN model over the last 30 years. Atmos. Chem. Phys. 14, 9317–9341. https://doi.org/10.5194/acp-14-9317-2014.

Skamarock, W.C., Klemp, J.B., Dudhia, J., Gill, D.O., Liu, Z., Berner, J., Wang, W., Powers, J.G., Duda, M.G., Barker, D.M., Huang, X.-Y., 2019. A description of the advanced research WRF model version 4. NCAR technical note NCAR/TN-556+STR. National Center for Atmospheric Research, Boulder, Colorado. https://doi.org/10.5065/1dfh-6p97.

Stockwell, W.R., Kirchner, F., Kuhn, M., Seefeld, S., 1997. A new mechanism for regional atmospheric chemistry modeling. J. Geophys. Res. 102, 25847–25879. https://doi.org/10.1029/97JD00849.

Sun, J., Ye, C., Liu, M., Wang, Y., Chen, J., Wang, S., Lu, X., Liu, G., Xu, M., Li, R., Liu, S., Zhou, H., Du, Z., Peng, F., Tsunekawa, A., Tsubo, M., 2022. Response of net reduction rate in vegetation carbon uptake to climate change across a unique gradient zone on the Tibetan Plateau. Environ. Res. 203, 111894. https://doi.org/10.1016/j.envres.2021.111894.

Surratt, J.D., Chan, A.W.H., Eddingsaas, N.C., Chan, M., Loza, C.L., Kwan, A.J., Hersey, S. P., Flagan, R.C., Wennberg, P.O., Seinfeld, J.H., 2010. Reactive intermediates revealed in secondary organic aerosol formation from isoprene. Proc. Natl Acad. Sci. U. S. A. 107, 6640–6645. https://doi.org/10.1073/pnas.0911114107.

Tian, Y., Wang, S., Jin, X., 2025. Global patterns and trends in ground-level ozone chemical formation regimes from 1996 to 2022. Atmos. Chem. Phys. 25, 9127–9149. https://doi.org/10.5194/acp-25-9127-2025.

Tie, X., Madronich, S., Walters, S., Edwards, D.P., Ginoux, P., Mahowald, N., Zhang, R., Lou, C., Brasseur, G., 2005. Assessment of the global impact of aerosols on tropospheric oxidants. J. Geophys. Res. Atmos. 110, D03204. https://doi.org/10.1029/2004JD005359.

van Geffen, J.H.G.M., Eskes, H.J., Boersma, K.F., Maasakkers, J.D., Veefkind, J.P., 2019. TROPOMI ATBD of the total and tropospheric NO_2 data products. S5P-KNMI-L2-0005-RP. Royal Netherlands Meteorological Institute, De Bilt, Netherlands. https://sentiwiki.copernicus.eu/_attachments/1673595/S5P-KNMI-L2-0005-RP%20-%20Sentinel-5P%20TROPOMI%20ATBD%20NO2%20data%20products%202024%20-%202.8.0.pdf.

Veefkind, J.P., Aben, I., McMullan, K., Förster, H., de Vries, J., Otter, G., Claas, J., Eskes, H.J., de Haan, J.F., Kleipool, Q., van Weele, M., Hasekamp, O., Hoogeveen, R., Landgraf, J., Snel, R., Tol, P., Ingmann, P., Voors, R., Kruizinga, B., Vink, R., Visser, H., Levelt, P.F., 2012. TROPOMI on the ESA sentinel-5 precursor: a GMES mission for global observations of the atmospheric composition for climate, air quality and ozone layer applications. Remote Sens. Environ. 120, 70–83. https://doi.org/10.1016/j.rse.2011.09.027.

Wang, H., Liu, X., Wu, C., Lin, G., 2024. Regional to global distributions, trends, and drivers of biogenic volatile organic compound emission from 2001 to 2020. Atmos. Chem. Phys. 24, 3309–3328. https://doi.org/10.5194/acp-24-3309-2024.

Wang, H., Wu, Q., Guenther, A.B., Yang, X., Wang, L., Xiao, T., Li, J., Feng, J., Xu, Q., Cheng, H., 2021. A long-term estimation of biogenic volatile organic compound (BVOC) emission in China from 2001–2016: the roles of land cover change and climate variability. Atmos. Chem. Phys. 21, 4825–4848. https://doi.org/10.5194/acp-21-4825-2021.

Wang, N., Liu, S., Xu, J., Wang, Y., Li, C., Xie, Y., Lu, H., Yang, F., 2025. Climate-driven biogenic emissions alleviate the impact of human-made emission reductions on O_3 control in the Pearl river Delta region, southern China. Atmos. Chem. Phys. 25, 8859–8870. https://doi.org/10.5194/acp-25-8859-2025.

Woo, J.-H., Kim, Y., Kim, H.-K., Choi, K.-C., Eum, J.-H., Lee, J.-B., Lim, J.-H., Kim, J., Seong, M., 2020. Development of the CREATE inventory in support of integrated climate and air quality modeling for Asia. Sustainability 12, 7930. https://doi.org/10.3390/su12197930.

Xavier, C., Rusanen, A., Zhou, P., Dean, C., Pichelstorfer, L., Roldin, P., Boy, M., 2019. Aerosol mass yields of selected biogenic volatile organic compounds—A theoretical study with nearly explicit gas-phase chemistry. Atmos. Chem. Phys. 19, 13741–13758. https://doi.org/10.5194/acp-19-13741-2019.

Xu, L., Pye, H.O.T., He, J., Chen, Y., Murphy, B.N., Ng, L.N., 2018. Experimental and model estimates of the contributions from biogenic monoterpenes and sesquiterpenes to secondary organic aerosol in the southeastern United States. Atmos. Chem. Phys. 18, 12613–12637. https://doi.org/10.5194/acp-18-12613-2018.

Zhang, H., Hu, Z., Chen, X., Li, J., Zhang, Q., Zheng, X., 2025. Global greening major contributed by climate change with more than two times rate against the history period during the 21th century. Glob. Change Biol. 31, e70126. https://doi.org/10.1111/gcb.70126.

Zhu, Z., Piao, S., Myneni, R.B., Huang, M., Zeng, Z., Canadell, J.G., Ciais, P., Sitch, S., Friedlingstein, P., Arneth, A., Cao, C., Cheng, L., Kato, E., Koven, C., Li, Y., Lian, X., Liu, Y., Liu, R., Mao, J., Pan, Y., Peng, S., Peñuelas, J., Poulter, B., Pugh, T.A.M., Stocker, B.D., Viovy, N., Wang, X., Wang, Y., Xiao, Z., Yang, H., Zaehle, S., Zeng, N., 2016. Greening of the Earth and its drivers. Nat. Clim. Change 6, 791–795. https://doi.org/10.1038/nclimate3004.